HHS Public Access

Author manuscript

Nano Lett. Author manuscript; available in PMC 2021 January 08.

Published in final edited form as:

Nano Lett. 2020 January 08; 20(1): 768–779. doi:10.1021/acs.nanolett.9b04876.

Overcoming diffusion-limited trapping in nanoaperture tweezers using opto-thermal-induced flow

Abhay Kotnala, **Pavana Siddhartha Kollipara**, **Jingang Li**, **Yuebing Zheng***

Walker Department of Mechanical Engineering, Material Science and Engineering Program and Texas Material Institute, The university of Texas at Austin, Texas 78712, USA

Abstract

Nanoaperture-based plasmonic tweezers have shown tremendous potential in trapping, sensing and spectroscopic analysis of nano-objects with single-molecule sensitivity. However, the trapping process is often diffusion-limited and therefore suffers from low-throughput. Here, we present bubble- and convection-assisted trapping techniques, which use opto-thermally generated Marangoni and Rayleigh-Bénard convection flow to rapidly deliver particles from large distances to the nanoaperture instead of relying on normal diffusion, enabling a reduction of 1–2 orders of magnitude in particle-trapping time (i.e., time before a particle is trapped). At a concentration of 2×10^7 particles/ml, average particle-trapping times in bubble- and convection-assisted trapping were 7 and 18 seconds, respectively, compared to 300 seconds in the diffusion-limited trapping. Trapping of a single particle at an ultralow concentration of 2×10^6 particles/ml was achieved within 2–3 minutes, which would otherwise take hours in the diffusion-limited trapping. With their quick delivery and local concentrating of analytes at the functional surfaces, our convection- and bubble-assisted trapping could lead to enhanced sensitivity and throughput of nanoaperture-based plasmonic sensors.

Graphical Abstract

***Corresponding Authors:** zheng@austin.utexas.edu.

Supporting information

Additional information on Gold nano-islands (AuNIs) substrate (Section A), Transmission spectrum of a single 300 nm circular nanoaperture in 100 nm Au film (Section B), Temperature rise in Au film with nanostructures: a comparative study (Section C), Demonstration of trapped and printed particles in a bubble-assisted trap (Section D), Contribution of trapping laser beam (1020 nm) to bubble generation and Rayleigh-Bénard convection (Section E), Bubble-assisted trapping of 100 nm polystyrene nanoparticles (Section F), Theoretical estimation of particle-trapping time for a diffusion-limited trap (Section G), Lateral flow velocity measurement in a convection-assisted trap (Section H) and Convection-assisted trapping of 100 nm polystyrene nanoparticles (Section I), SEM image of an AuNIs-encapsulated nanoaperture (Section J), Supplementary Notes 1 and 2.

The authors declare no competing financial interest.

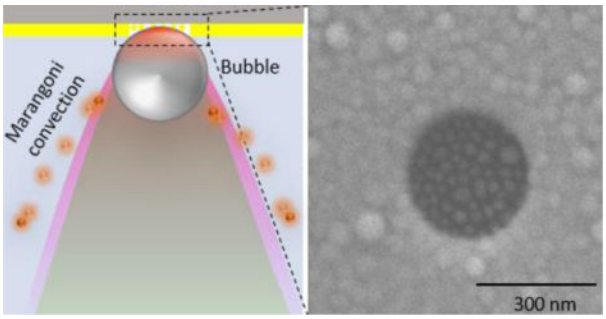

Keywords

Optical trapping; Plasmonic tweezers; Convection flow; Nanoaperture; Marangoni convection

INTRODUCTION

Nanoaperture-based plasmonic tweezers (NAPTs) are promising for single-nanoparticle trapping, sensing and spectroscopy.[1–10] By focusing light below the diffraction-limit and providing enhanced light-matter interactions, plasmonic nanoapertures have enabled stable trapping of sub-100 nm particles like quantum-dots[11], proteins[12], and DNA[13,14]. Furthermore, nanoapertures can enhance the fluorescence[15–18], Förster resonance energy transfer[19,20], second-harmonic generation[21,22] and Raman signal of the trapped nanoparticles[23–25]. When formed into arrays, nanoapertures can lead to extraordinary optical transmission.[26] Single-nanoparticle trapping and signal-enhancement capabilities of NAPTs have led to their uses in studies of protein dynamics[27], protein-small-molecules interactions[28] and protein-DNA interactions[29], protein characterization[30], biosensing[31,32] and spectroscopy[33,34]. With emergence of novel nanoaperture designs, simple nanoaperture fabrication strategies[35,36] and their integration with microfluidics[37] and nanopore[38], NAPTs are expanding their applications. However, trapping or sensing of nanoparticles using nanoapertures suffer from an intrinsic problem of low-throughput as the particle-delivery process is often diffusion-limited. In other words, it often takes long time for particles to diffuse into close proximity (usually within tens of nm) of nanoapertures before they can be trapped or detected due to the short-range plasmon-enhanced electromagnetic fields at the nanoapertures[39]. The trapping time increases substantially for low-concentrated samples such as HIV virions in human blood[40] where the diffusion-limited trapping of a single HIV particle at the plasmonic nanoaperture could take several hours.

One solution to this diffusion-limited problem in optical tweezers is the integration of the tweezers with flow-fields where particles are quickly delivered to the trapping region via liquid or air flow instead of normal diffusion. For example, an aerodynamic system consisting of a counter-flow coaxial-double-nozzle was integrated with optical tweezers to continuously deliver air-borne particles to the optical trapping region[41]. For particles suspended in liquids, optical tweezers were integrated with spatially confined microfluidic channels where the laminar flow in the channels quickly delivers particles to the trapping region and the small channel cross-section maximizes the particle-trapping probability.[42] However, extending this flow-based approach to NAPTs is limited by complex fabrication

and integration of plasmonic nanoapertures with nanofluidic channels. Another approach that exploits electric field to transport particles to plasmonic tweezers is only applicable to charged particles in an ionic solution and suffers from the requirement for precise fabrication of nanopores at the electromagnetic hotspot of plasmonic nanoantenna or nanoaperture[43,44]. Recently, electro-thermo-plasmonic (ETP) effect has been used for long-range and rapid delivery of nanoparticles to plasmonic nanoantennas for particle trapping[45] and sensing.[46] Such ETP systems use thermal gradient and electrical field to create strong particle flow directed towards the hot region in the solution. However, the ETP flow associated with the small temperature gradient that is opto-thermally generated at a single plasmonic nanoaperture is not strong enough for effective particle delivery.[47] Despite their capability of creating strong ETP flows, nanoaperture arrays often result in ensemble particle trapping or agglomeration of particles.

In this work, we demonstrate that opto-thermally generated Rayleigh-Bénard convection and bubble-induced Marangoni convection can be exploited to overcome the diffusion-limited trapping in plasmonic tweezers based on single nanoapertures. The fluid flow induced by Rayleigh- Bénard convection or Marangoni convection can quickly deliver particles over large spatial distances to the plasmonic nanoaperture for the trapping. We refer to the trapping system using the Rayleigh-Bénard convection as a convection-assisted trap and the one using the bubble-induced Marangoni convection as a bubble-assisted trap. A trapping system where the particles encounter the nanoaperture through normal diffusion is termed as a diffusion-limited trap. Our convection-assisted traps have enabled a reduction of 1–2 orders of magnitude in particle-trapping time compared to that of a diffusion-limited trap. The integration of opto-thermal-induced flow with NAPTs does not require complex fabrication of nanofluidic channels or use of external electric fields as the flow can be optically generated and directed towards the laser spot in a simple solution chamber. Moreover, both convection- and bubble-assisted traps can be implemented with a single nanoaperture to trap single particles at a time rather than an ensemble of particles as demonstrated earlier.[46] As a discrete process, bubble-assisted trapping requires generation and collapse of a microbubble for the delivery and trapping of a particle. Convection-assisted trapping is a continuous process where particle can be trapped and released continuously upon the generation of convection flow. The convection and bubble-assisted trapping processes can be applied to nanoapertures of any shape and size to improve both detection limit and throughput of plasmonic sensors.[48]

WORKING PRINCIPLE AND EXPERIMENTAL SET-UP

I. Bubble-assisted trap

Opto-thermally generated bubbles were used to capture[49,50] or print[51] particles on substrates and to control fluid flow in microfluidic devices[52] using Marangoni convection and gas pressure generated by the bubble. A bubble-assisted trap uses an optically controlled microbubble generated at the plasmonic nanoaperture to create both natural convection and Marangoni convection in the solution chamber. The natural convection arises from the density gradient of the fluid as a result of localized heating at the nanoaperture. The Marangoni convection is induced by surface tension gradient along the microbubble surface,

which leads to rapid flow and capture of particles at the bubble-water interface. The particles can be delivered to the bubble from distances as far as 200 μm with velocities ranging from 10 μm/s to 100 mm/s[53]. Once the particles are captured at the interface, the bubble is collapsed immediately upon withdrawing of the laser beam. Consequently, the particles get pulled towards the nanoaperture along the bubble-water interface and ultimately get trapped at the nanoaperture by the plasmon-enhanced optical forces. Thus, the bubble-induced flow significantly reduces the travel time of the particles to the nanoaperture.

However, opto-thermal generation of bubbles with nanoapertures on gold (Au) films is challenging. This is due to the high thermal conductivity of Au layer, which quickly dissipates the heat and thus prevents localized heating at the nanoaperture that is needed to raise the temperature of nanoaperture above 100°C for bubble generation. To overcome the challenge, we fabricated nanoapertures on a gold nano-islands (AuNIs) substrate (See Supporting Information: Section A), leading to nanoapertures with embedded AuNIs, which are termed as AuNIs-encapsulated nanoapertures as shown in Figure 1a (See METHODS section for fabrication details). AuNIs provide strong light absorption at a wavelength of 532 nm and high opto-thermal conversion efficiency for bubble generation using relatively low optical power[51]. The AuNIs-encapsulated nanoapertures were stable and repeatedly used for bubble generation and trapping of particles for the laser intensity used in our experiments (See Supporting Note 1). Heat equations were solved using commercially available finite-element solver (See METHODS section) to obtain the temperature distribution around a 10 μm bubble generated in a bubble-assisted trap as shown in Figure 1b. The bubble was generated by illuminating an AuNIs-encapsulated nanoaperture with a focused laser beam of a diameter of 2 μm and power intensity of 3 mW/μm^2. The temperature is maximum at the bubble-substrate interface (370 K) and decreases to 310 K at the top of the bubble due to the localized heating that arises from optical absorption of the AuNIs. The temperature difference of ~ 60 K between the top and bottom of the bubble creates a mean surface tension gradient of 0.167 mN/m.K along the bubble surface, which leads to a flow distribution around the bubble as shown in Figure 1c. The flow velocities range from 100 μm/s to 100 mm/s within a span of 100 μm from the microbubble, consistent with the experimental measurements reported in the literature[53]. The flow with its trajectory directed towards the nanoaperture can deliver particles from distances as far as 200 μm with spatially varying velocities.

A 532 nm laser beam (diode-pumped solid-state laser, Genesis MX STM-1 W; Coherent) was used for generation of the bubble. An additional laser operating at a wavelength of 1020 nm (diode-pumped Ytterbium fiber laser, YLM-1, IPG Photonics) was used for plasmonic excitation of the nanoaperture to trap the flow-delivered nanoparticles. A nanoaperture of a diameter of 300 nm on a 100 nm-thick Au film was chosen for the trapping demonstration since its optical transmission cut-off wavelength at ~ 990 nm in solution was close to the trapping laser wavelength (i.e., 1020 nm)[2]. The simulated optical transmission spectrum of the nanoaperture is shown in Supporting Information: Section B. The schematic of the experimental set-up for bubble-assisted trapping is shown in Figure 1d where the two laser beams are co-incident and focused on an AuNIs-encapsulated nanoaperture using a 100× oil immersion objective lens (NA=1.3). A halogen lamp was applied for fluorescence excitation

of polystyrene nanoparticles that were used along with a charge-coupled device (CCD) for visualization of the trapping process.

II. Convection-assisted trap

Bubble-assisted trapping requires generation and collapse of a bubble every time when a particle need be trapped by the nanoaperture. While it can quickly deliver particles to the nanoaperture trap site and reduce the trapping time, the on/off nature of flow results in a discrete trapping process rather than a continuous one where particles can be trapped continuously in a flow environment. A convection-assisted trap exploits the Rayleigh-Bénard convection flow to rapidly and continuously transport particles into the vicinity of a nanoaperture where they get trapped. The trapping of particles can occur continuously without turning off the flow.

Fluid can be set into motion by creating a temperature gradient in the solution, which produces buoyancy-driven natural convection due to the fluid's density gradient as a function of temperature. Due to their strong dissipative loss and opto-thermal conversion efficiency that leads to a substantial increase in local temperature, plasmonic nanostructures have been successfully used to create convection flow in a solution chamber.[54] However, the convection is too weak to create high flow velocities due to the concentration of temperature distribution to a small area at the plasmonic nanostructure that prevents effective transduction of heat to the fluid. Even heating to high temperatures near the boiling point of water results in weak convection flow velocities of the order of a few 100 nm/s.[55] Given that the buoyancy force is dependent on the spatial temperature distribution, heating of a large area can help achieve high convection velocities. For example, plasmonic nanostructure arrays on an ITO substrate increased the spatial temperature distribution and thus the convection flow velocities to a few μm/s.[56] The velocity of the fluid (V) induced by a plasmonic structure of a dimension of L and temperature increase T_o is given by[55]

$$V = L^2 \beta g T_o / \nu$$

where L is the characteristic length of the structure, β is the dilation coefficient of water, g is the gravitational acceleration, T_0 is the temperature increase and ν is the viscosity of water. The convection flow velocity has a linear dependence on the temperature rise of the structure and quadratic dependence on the structure dimension. The heat influx into fluid depends linearly on the temperature increase and area of the structure-fluid interface. We exploit the dependence to induce strong convection flow in the nanoaperture tweezers.

Instead of heating a localized area at the nanoaperture using a focused laser beam, which resulted in temperature rise with a limited spatial distribution, we illuminated a large area (diameter > 50 μm) of Au film around the nanoaperture using a multimode (MM) optical fiber as shown in Figure 2a. The illumination of a large area effectively distributes the thermal energy and increases the spatial extent of the temperature distribution, resulting in a strong Rayleigh-Bénard convection flow in the solution chamber. We solved heat equations using a commercial finite-element solver (See METHODS section) to obtain the temperature distribution at the Au surface around the nanoaperture as shown in Figure 2b. The Au layer

around the nanoaperture was illuminated over an area of a diameter of 60 μm with a 532 nm laser beam of a power intensity of 0.02 mW/μm^2. A temperature rises of ~ 40 °C above room temperature (20 °C) occurs at the Au surface in contact with the solution, which results in Rayleigh-Bénard convection within the solution chamber. The temperature rise is larger than that reported in literature for Au films with nanostructures[57–59] due to the illumination of the larger-area Au film that leads to the higher optical absorption and conversion into heat (See Supporting Information: Section C).

The flow velocity distribution resulting from the Rayleigh-Bénard convection was obtained using the computational fluid dynamics (CFD) simulations (See METHODS section for details) and displayed in Figure 2c. The flow velocity distribution is a complex vector field, which dictates the trajectory of particles in the convection flow. For flow trajectories directed towards the nanoaperture, convection flow can transport particles from lateral distances of more than 100 μm towards the vicinity of the nanoaperture with a velocity of 20 μm/s. While certain flow trajectories transport particles from the bulk solution towards the nanoaperture, the flow at the nanoaperture tends to drive particles away from the nanoaperture. However, if the flow velocity at the nanoaperture is not large enough to create a drag force larger than the trapping force, particles can be transported quickly from the bulk solution towards the nanoaperture and get trapped, thereby reducing the particle trapping time. At a certain cut-off flow velocity when the drag force becomes larger than the trapping force, trapping of particles would be impossible using a convection-assisted trap. Thus, it is important to study the impact of convection flow velocity at the nanoaperture on the particle trapping time and to estimate the cut-off flow velocity beyond which the convection-assisted trapping stops functioning as discussed in the later section.

Figure 2d shows the schematic of the experimental set-up used for convection-assisted trapping. An MM optical fiber with a 532 nm incident laser beam was used to generate the convection flow in the solution chamber. The light from the MM fiber was incident from the substrate side and positioned just above the nanoaperture, which was used for trapping the particles as illustrated in the enlarged section of Figure 2d. An objective lens can also be used instead of an MM fiber to illuminate the Au surface surrounding the nanoaperture, but it might require slight defocusing with respect to the Au layer to increase the illumination spot to a larger size. A 1020 nm laser beam was focused on the nanoaperture from the solution side to achieve trapping of particles in the presence of convective flow as shown in Figure 2d. The 1020 nm laser has a negligible impact on the convection flow velocity, which is mainly controlled by modulating the output power of the MM fiber. A circular nanoaperture of a diameter of 300 nm was used to demonstrate the trapping of 200 nm polystyrene particles in a continuous convection-flow environment.

RESULTS AND DISCUSSION

I. Bubble-assisted trapping

The experimental set-up shown in Figure 1d was used to demonstrate the bubble-assisted trapping of particles. It is a two-step serial process. The first step involves the generation of an opto-thermal bubble and the second step involves plasmonic trapping of particles. Figures 3(a–g) show representative time-lapsed images of bubble-assisted trapping of a single 200

nm fluorescent polystyrene particle using a single circular nanoaperture (See Supporting Video 3). Initially, when both lasers were turned “OFF” (T= 0 sec), the nanoparticles freely diffused in the solution chamber. To start the bubble-assisted trapping process, both laser beams were turned “ON” simultaneously at T= 2.04 seconds. The 532 nm laser beam generated the bubble, resulting in Marangoni convection due to which the particles were rapidly driven towards the bubble and captured at the bubble-water interface as shown in Figure 3c. Two particles were captured at the bubble-water interface as shown in Figure 3d. However, the number of particles captured at the bubble-water interface can vary from single to multiple particles depending on the duration for which 532 nm laser is switched “ON”, particle concentration and instantaneous distribution of particles.

The 532 nm laser was turned-off immediately after bubble generation (typically within 1–2 seconds) following which the bubble starts collapsing as shown in Figures 3(c–e). For effective bubble-assisted trapping, it is important to control the 532 nm laser “ON” time (or bubble-on-time) so that most of the particles are only driven and captured at the bubble-water interface. A longer laser on-time increases the chance of some of the particles getting immobilized on the substrate rather than being captured at the bubble-water interface. The laser “ON” time of 1–2 seconds was found to be sufficient to capture some of the particles at the bubble-liquid interface without getting immobilized on the substrate. We observed that high particle concentrations or laser “ON” time greater than 1–2 seconds could print particles on the substrate surface close to the bubble (See Supporting Information: Section D and Supporting Video 4).

The 1020 nm trapping laser beam, which is kept “ON” during this process, does not influence the bubble generation and collapse dynamics as it does not contribute to the heating of the nanoaperture due to the minimal light absorption by AuNIs at an off-resonance wavelength. The negligible contribution of 1020 nm laser to bubble generation and dynamics, i.e., the growth and collapse of bubble, was verified experimentally through our control experiments (See Supporting Information: Section E). A minimum laser intensity of 3 $mW/\mu m^2$ was needed for bubble generation and the trapping laser intensity was 1.6 $mW/\mu m^2$. The typical bubble sizes were in the range of 10–20 μm, which collapsed in less than 10 seconds after the 532 nm laser was turned “OFF”. During the bubble collapse, the particles were dragged along the bubble-water interface towards the nanoaperture. The particles got trapped at the nanoaperture once the bubble collapsed completely as shown in Figures 3f. We observed that a single nanoparticle was trapped in about five seconds after the generation of the bubble. To confirm that the nanoparticle was optically trapped rather than being printed at the nanoaperture, we turned “OFF” the 1020 nm laser after 8 seconds, which resulted in the release of the nanoparticle from the nanoaperture as shown in Figure 3g. A new bubble need be generated in order to transport and trap another particle.

Besides direct observation of the particle-trapping process on a CCD camera, we employed time trace of light intensity at the nanoaperture to further reveal the trapping dynamics as shown in Figure 3h (See Supporting Note 2). Bubble-assisted trapping was also performed with polystyrene particles of 100 nm in diameter (See Supporting Information: Section F and Supporting Video 5) to show the versatility of this technique in trapping the smaller-

sized particles. Successful delivery and trapping of a nanoparticle will be achieved as long as the optical forces at the nanoaperture are strong enough to capture the nanoparticle. To trap the much smaller particles, one could implement bubble-assisted trapping with the more complex nanoapertures such as bowtie[4], double-nanohole[3] or coaxial[12], which could trap tiny nanoparticles of down to few tens of nm with high trapping stiffness.

To quantify the reduction in particle-trapping time provided by the bubble-assisted trap in comparison to a diffusion-limited trap, we measured the average trapping time of particles for both processes at different particle concentrations. The particle-trapping time in a bubble-assisted trap corresponds to the time interval between the excitation of the bubble and the trapping of a particle. For a diffusion-limited trap, it was measured from the point the trapping laser was turned “ON” till the trapping of a particle. Multiple trapping events were recorded to determine the average trapping time for each case. Figure 3i shows the comparison of the average trapping time for bubble-assisted and diffusion-limited trap at three different particle concentrations of 2×10^9, 2×10^8 and 2×10^7 particles/ml. These concentration levels are more than two orders-of-magnitude lower than the concentrations of particles that have typically been used in various nanoaperture tweezers experiments[1,2,12] and are suitable to demonstrate the effectiveness of bubble-assisted trap in reducing the particle-trapping time compared to a diffusion-limited trap. In addition, the concentration range used in the experiments is of practical significance as many nanoparticles of biological significance such as exosomes extracted from body fluids[60], viruses in human blood[61] and cancer biomarkers in human fluid[62] lie within this range.

As shown in Figure 3i, the average trapping time in a bubble-assisted trap was reduced by ≈ 60- and 40-fold for concentrations of 2×10^9 and 2×10^8 particles/ml, respectively. For the low concentration of 2×10^7 particles/ml, few trapping events were observed for the diffusion-limited trap within the maximum data-collection time of 600 seconds. However, bubble-assisted trapping reduced the average trapping time to only 7 seconds. We also theoretically estimated the average particle-trapping time for a diffusion-limited trap, which correlated well with our experimental observation (See Supporting Information: Section G). We further tried to push the bubble-assisted trap for trapping particles at an ultra-low concentration of 10^6 particles/ml. However, the short bubble-generation time of 1–2 seconds was not enough to drive the particles to the bubble-water interface due to a low probability of presence of particles within the flow field of the bubble at any instant. As a result, the bubble had to be turned on for a long time (> 10 s) so that the particles could diffuse into the bubble’s flow field, which were then driven to the bubble-water interface.

The long and indeterministic bubble-on-time led to a poor control of particle flow to the bubble and, in most cases, resulted in printing of the particle on the substrate surface rather than getting captured at the bubble-water interface. Thus, trapping of particles could not be carried out at such ultra-low concentrations. A possible solution to avoiding printing or immobilization of the particles on the substrate during the bubble-assisted trapping might be hydrophilic surface modification of the Au surface using self-assembled monolayers of hexanethiol[63], propanethiol[64] and mercaptoundecanoic acid[65], which have been found to be stable up to 375–500 K.

II. Convection-assisted trapping

To initiate the convection-assisted trapping, the output laser beam from the MM fiber was aligned with the nanoaperture such that it illuminated a considerably large Au surface area around the nanoaperture. The output intensity of the MM fiber was set at 0.02 mW/μm^2 to initiate the Rayleigh-Bénard-convection-induced flow in the solution chamber containing the nanoparticles. Simultaneously, the 1020 nm laser was turned “ON” and focused on the nanoaperture using a 40×objective lens to achieve trapping of particles in the convection flow. The 1020 nm trapping laser has a negligible contribution to the Rayleigh-Bénard convection flow, which was verified through control experiments (See Supporting Information: Section E). Some of the particles that had been driven to the proximity of the nanoaperture were trapped while others flew away from the nanoaperture due to the convective current (See Supporting Video 6).

Figures 4(a–g) show the time-lapsed images of trapping of a single 200 nm fluorescent polystyrene particle in a convection-assisted trap. The nanoparticle was optically trapped at the nanoaperture at T=3.45 s for a duration of approximately half a second before it was released by turning “OFF” the 1020 nm trapping laser (Figure 4d). The time-lapsed images are shown only from T=2.65 s to T=4.55 s as the particle position could be accurately tracked only during this period. At other times, the particle was way out of focus of the optical microscope due to its motion in the Z direction (see Figure 2d) during the convection flow, making it challenging to optically track the position of the particle. The arrows in Figures 4(a–g) point to the location of the particle in the convection flow. Trapping in a convection-assisted trap was a continuous process and individual particles were trapped continuously one after another in the presence of a steady convective flow (See Supporting Video 6). Figure 4h shows the time trace of light intensity at the nanoaperture during a convection-assisted trapping process. Whenever a particle is trapped at the nanoaperture, it can be detected from the increase in light intensity at the nanoaperture due to the fluorescence excitation of the trapped particle by the 532 nm laser beam transmitted through the nanoaperture. Multiple bursts in intensity correspond to the trapping and release of multiple particles in the convection flow. Upon being trapped, the particles were released immediately (typically in less than a second) so that only a single particle could be trapped continuously at the nanoaperture. However, there may be instances when a particle enters the trap before the previously trapped particle is released, resulting in trapping of multiple particles at the nanoaperture. Such rare events were clearly identified in the time trace of light intensity at the nanoaperture, which showed the larger intensity change in comparison to a single trapped particle due to the additional fluorescence signal from the extra particles. For example, at time ~ 28 seconds in Figure 4h (and Supporting Video 6), we observe a change in light intensity at the nanoaperture that is 20% higher than other bursts of almost similar intensities, indicating trapping of more than one particle at the nanoaperture. Convection-assisted trapping process was carried at an average lateral convection-flow velocity of ~ 20 μm/s in the vicinity of the nanoaperture (See Supporting Information: Section H). The flow velocity matches that obtained from the CFD simulations for the given incident laser intensity (Figure 2c).

Similar experiments were performed using 100 nm polystyrene particles to demonstrate that convection-assisted trapping can work for the smaller-sized particles (See Supporting Information: Section I). However, stable trapping of the smaller particles using a convection-assisted trap becomes increasingly challenging due to a significant reduction in near-field optical gradient force that scales with particle volume, making it difficult for optical forces to overcome both the drag force and Brownian motion of the particle.

To demonstrate that convection-assisted trap can overcome the diffusion-limited trapping in nanoaperture tweezers, we compared the average particle-trapping time in a convection-assisted trap to that of a diffusion-limited trap. To obtain average particle-trapping time in a convection-assisted trap, multiple particles were trapped and released continuously in a convection flow and the time interval between two consecutive trapping events was recorded. The time intervals correspond to the particle-trapping time and were used to calculate the mean particle-trapping time. Figure 4i shows the comparison of the average particle-trapping time between a convection-assisted and a diffusion-limited trap at three different concentrations of particles. The average trapping time was reduced by five-fold and fifteen-fold for particle concentrations of 2×10^8 and 2×10^7 particles/ml, respectively. For an ultra-low concentration of 2×10^6 particles/ml, few trapping events were observed in a diffusion-limited trap within the data collection time of ~ 600 seconds. However, convection-assisted trap reduced the average trapping time to 128 seconds. All the experiments at the different concentrations were performed with an average convection flow velocity of ~ 20 μm/s at the nanoaperture (See Supporting Information: Section H). The convection-assisted trapping significantly reduced the average particle-trapping time compared to a diffusion-limited trap and brought trapping time within practically reasonable limits of a few minutes for ultra-low concentration of 2×10^6 particles/ml, which would have otherwise taken hours in a diffusion-limited trap.

III. Impacts of flow velocity and laser power in a convection-assisted trap

We further studied the impacts of flow velocity and laser power on the average particle-trapping time in a convection-assisted trap. Experiments were conducted to determine the variation in the average particle-trapping time with an increase in convection-flow velocities. The convection-flow velocity was increased by increasing the optical power incident on the Au surface surrounding the nanoaperture, which caused a rise in the temperature of the Au surface and the higher convection flow velocities. For these experiments, the concentration of particles in the solution and the trapping laser power intensity were kept constant at 2×10^7 particles/ml and 1.28 mW/μm^2, respectively. We choose this particle concentration because it lies within the range of concentrations used in the convection-assisted trapping experiments described in the above section. In addition, due to the relatively lower particle-trapping time at this concentration, it is easier to collect large data set for different flow velocities in short time. However, we believe that the qualitative behavior of the outcome of this study would remain unaffected even if the experiment was conducted with different particle concentrations (e.g., 2×10^8 particles/ml). A change in particle concentration would not change the trend of the dependence of the trapping times on the flow velocities but modify the absolute values of the particle-trapping times.

Figure 5a shows that the average particle-trapping time reduces as the convection-flow velocity is increased. This is because high flow velocity can speed up the delivery of particles to the nanoaperture and therefore reduce the trapping time. In principle, the higher the convection flow velocity, the smaller the particle-trapping time. However, the flow velocity cannot be increased beyond a limit because, above a certain threshold, it creates a strong Stokes drag force on the particle that is large enough to overcome the trapping potential provided by the nanoaperture trap and to result in no trapping of particles. In our experiments, we observed no trapping of particles for convection-flow velocities above ~ 50 μm/s at the nanoaperture, suggesting an increase in drag force past the trapping potential of the nanoaperture trap at the given trap laser intensity. This puts an upper bound on the convection-flow velocities that can be used in a convection-assisted trap, which depends on the trapping stiffness of nanoaperture tweezers at given laser intensities. It should be noted that the number of trapping events within a given time frame varies for different flow velocities due to the scaling in particle-trapping time with convection flow velocities. For example, the higher flow velocities result in the lower average particle-trapping time and hence the larger number of trapping events recorded in a given time.

During the convection flow, the particle trapped at the nanoaperture experiences a drag force that pushes the particle away from the nanoaperture. A strong trapping force greater than the drag force is needed to trap the particle at the nanoaperture. Due to the competitive nature of the Stokes drag force and the trapping force, the magnitude of the trapping potential provided by the nanoaperture also impacts the average particle-trapping time in a convection-assisted trap. Since the trapping potential is directly related to the trap laser intensity, experiments were conducted to determine its impact on the average particle-trapping time in a convection-assisted trap. Figure 5b shows the variation in average trapping time as the trap laser intensity was increased. For these experiments, the concentration of particles was fixed at 2×10^8 particles/ml and a steady convection-flow was maintained by a constant output laser power from the MM fiber. Since our previous study was performed at the particle concentration of 2×10^7 particles/ml, we purposely performed this study at 2×10^8 particles/ml to demonstrate that any concentration of particles can be used for these parametric studies without affecting the general conclusions.

Briefly, the average particle-trapping time reduces as the trap laser intensity increases. The increase in trap laser intensity increases the trapping stiffness, a well-known fact for optical tweezers, and therefore increases the probability of trapping of particles encountered by the nanoaperture as is evident at trap power intensity of 1.28 $mW/\mu m^2$ (Figure 5b). When the trap laser intensity is decreased, the trap stiffness reduces, causing a decrease in the probability of trapping of particles in the flow and thus an increase in the average particle-trapping time. The average particle-trapping time was increased by three-fold as the trap laser power intensity decreased from 1 $mW/\mu m^2$ to 0.84 $mW/\mu m^2$ (Figure 5b). The increased trapping time could be attributed to a decrease in probability of trapping of particles due to a decrease in the trapping force that made it comparable to the drag force from the convection flow. For trap-laser intensity lower than 0.84 $mW/\mu m^2$, no trapping was observed, which suggests that the trapping force was not sufficient to overcome the drag force due to the convection flow.

IV. Comparison of bubble- and convection-assisted trap

Table 1 provides a summary of the comparison of the sample design, flow mechanism and trapping process of bubble- and convection-assisted trap. Our experimental results demonstrate that both bubble- and convection-assisted trap can significantly reduce the average particle-trapping time compared to a diffusion-limited trap in nanoaperture tweezers. However, the trapping of particles was found to be faster in a bubble-assisted trap compared to a convection-assisted trap at similar nanoparticle concentrations. This is due to the high flow velocities and unique flow profiles created by Marangoni convection in a bubble-assisted trap, which quickly transport majority of the suspended particles towards the nanoaperture. On the other hand, Rayleigh-Bénard convection created in a convection-assisted trap results in comparatively slow average flow velocities, which are at least an order of magnitude smaller than those due to Marangoni convection within a lateral span of 100 μm from the nanoaperture, and a flow profile, which results in particle trajectories that transport only limited number of particles to the nanoaperture vicinity while driving away some of the particles before their reaching the nanoaperture. Both the slow flow velocities and the transport of limited number of particles to the nanoaperture lead to a rise in particle-trapping time.

In addition, the flow velocities generated in a convection-assisted trap are limited by the trapping force provided by the nanoaperture tweezers, which is not the case in a bubble-assisted trap. The limit is due to the continuous trapping process in a convection-assisted trap where particles are trapped continuously in the presence of convection flow. The continuous flow imparts a drag force on the particle in a direction opposite to the optical trapping force from the nanoaperture, which need be balanced to observe the trapping of particles. This is in contrast to the discrete trapping process in a bubble-assisted trap where the flow of nanoparticles to the nanoaperture and the trapping of the particles occur serially independent of each other and no drag force acts on the particles during the trapping.

While both bubble- and convection-assisted trapping mechanisms are generally applicable to any nanoaperture tweezers, it may be beneficial to use one instead of the other based on the specific experimental conditions. For example, in case of nanoaperture designs with low trap stiffness or when trapping small Rayleigh particles for which the optical gradient forces reduce significantly, it is better to use bubble-assisted trap. Unlike convection-assisted trap, the optical forces do not need to overcome an additional drag force along with the Brownian motion in order to trap a particle in the bubble-assisted trap. However, for nanoaperture designs with high trapping stiffness that can easily overcome the convection-flow-induced drag force on the particles, a convection-assisted trap might be a better option as it can trap particles continuously in an automated and high-throughput fashion.

CONCLUSION

We developed bubble- and convection-assisted trapping techniques to overcome the diffusion-limited trapping in nanoaperture-based plasmonic tweezers. Both techniques reduced the average particle-trapping time by more than an order-of-magnitude compared to a diffusion-limited trap. In the case of ultra-low concentration samples (e.g., 2×10^6 particles/ml), the particle-trapping time changed from hours in a diffusion-limited trap to a few

minutes. With their simplicity and general applicability, the opto-thermal techniques can be easily integrated with all sorts of nanoaperture tweezers. In addition to increasing the throughput of nanoaperture tweezers, the opto-thermal-induced flow used in convection- and bubble-assisted traps could also be applied to enhance performance of nanoaperture-based plasmonic sensors[66]. The flow created by both techniques could rapidly deliver analytes with an increased concentration to the functional surfaces of the sensors, improving the sensitivity and throughput.

METHODS

Fabrication of AuNIs-encapsulated nanoapertures:

The AuNIs-encapsulated nanoapertures were fabricated using colloidal lithography. Firstly, glass substrates with AuNIs were fabricated by depositing Au thin films of thickness of 4.5 nm on glass slides (Denton thermal evaporator, base pressure: 9×10^{-6} torr, deposition rate: 0.1 Angstrom/s), followed by thermal annealing using a box furnace (Thermo Scientific™ Lindberg/Blue M™ Box Furnace) at 550 °C in air for 2 hours. Polystyrene particles with a diameter of 300 nm were spin-coated on the glass substrate with AuNIs followed by thermal deposition of 5 nm chromium and 100 nm Au film (Denton thermal evaporator, base pressure: 9×10^{-6} torr, deposition rate: 0.5 Angstrom/s). Polystyrene particles were then removed using a scotch tape, leaving behind AuNIs-encapsulated nanoapertures. The method can be used to form nanoaperture of any size and shape by using colloidal particles of corresponding size and shape as masks. For example, nanorods or nano-prisms could be used to fabricate rectangular or triangular nanoapertures. A dimer of spherical nanoparticles was used to fabricate double-nanohole apertures, which we also observed during our fabrication (See Supporting Information: Section J)[36]. Fabrication of more complex nanoapertures using colloidal lithography would require directed assembly for precise arrangement of multiple colloidal nanoparticles in an arbitrary fashion.[67–72]

Materials:

200 nm fluorescent polystyrene nanoparticles in solutions (excitation/emission wavelengths: 540/600 nm) used in the trapping experiments were prepared by diluting the as-purchased solutions (Bang Laboratories) in de-ionized water to reach final concentrations of 2×10^9, 2×10^8, 2×10^7, and 2×10^6 particles/ml.

SEM Characterization:

The high-resolution SEM image of the AuNIs-encapsulated nanoaperture in Figure 1a was taken using the FEI Quanta 650 ESEM.

Finite-Difference Time-Domain (FDTD) Simulations:

The three-dimensional electromagnetic simulation to determine the transmission cut-off wavelength of the nanoaperture was performed using a commercial software (FDTD Solutions, Lumerical Solutions). The design consisted of a single nanoaperture of a diameter of 300 nm in a 100 nm-thick Au film on a glass substrate embedded in water. The optical constants of Au were taken from Johnson and Christy[73] and the refractive index of the glass

substrate was set as 1.52. Perfectly matched layers were utilized as the boundary conditions for all directions.

Numerical Computational Fluid Dynamics (CFD) Simulations:

Coupled heat equations and Navier Stokes equations were solved for temperature and flow velocity, respectively, using a commercial finite-element solver (COMSOL Multiphysics V5.4). A two-dimensional axisymmetric model comprising of a glass substrate with a 100 nm-thick Au film, a microbubble, and water was established. Using pre-existing modules of “heat transfer in solids” and “conjugate heat transfer in fluids” along with “laminar flow” using “non-isothermal coupling”, Rayleigh-Bénard convection was simulated for the convection-assisted trap. For the bubble-assisted trapping, “Marangoni effect” was included in addition to the above modules to simulate the flow due to surface tension gradient along the bubble-water interface. Due to small chamber thickness of ~120 μm and convection flow velocities in the range of ~10–70 μm/s, the Reynolds number of the system was small (~ 0.01) and therefore resulted in a laminar flow. The boundary conditions considered for the heat transfer were composed of a volumetric heat source within the gold film to model the absorption due to laser heating and room temperature for other boundaries. For the laminar flow physics, the water/bubble interface was set as a slip interior wall, while the other boundaries were set as non-slip walls.

Supplementary Material

Refer to Web version on PubMed Central for supplementary material.

Acknowledgement

We acknowledge Youngsun Kim for helpful discussions during writing of the manuscript.

Funding Sources

A.K, P.S.K, J.L and Y.Z. acknowledge the financial supports of the National Science Foundation (NSF-CMMI-1761743), the National Aeronautics and Space Administration Early Career Faculty Award (80NSSC17K0520), and the National Institute of General Medical Sciences of the National Institutes of Health (DP2GM128446).

REFERENCES

(1). Kwak E; Onuta T; Amarie D; Potyrailo R; Stein B; Jacobson SC; Schaich WL; Dragnea B Optical Trapping with Integrated Near-Field Apertures. J. Phys. Chem. B 2004, 108, 13607–13612.

(2). Juan ML; Gordon R; Pang Y; Eftekhari F; Quidant R Self-Induced Back-Action Optical Trapping of Dielectric Nanoparticles. Nat. Phys 2009, 5, 915–919.

(3). Kotnala A; Gordon R Quantification of High-Efficiency Trapping of Nanoparticles in a Double Nanohole Optical Tweezer. Nano Lett. 2014, 14, 853–856. [PubMed: 24404888]

(4). Berthelot J; Aćimović SS; Juan ML; Kreuzer MP; Renger J; Quidant R Three-Dimensional Manipulation with Scanning near-Field Optical Nanotweezers. Nat. Nanotechnol 2014, 9, 295–299. [PubMed: 24584272]

(5). Prasad A; Choi J; Zheng J; Park S; Gartia MR Nanohole Array Plasmonic Biosensors : Emerging Point-of-Care Applications. Biosens. Bioelectron 2019, 130, 185–203. [PubMed: 30738247]

(6). Jiang J; Wang X; Li S; Ding F; Li N; Meng S; Li R; Qi J; Liu Q; Liu GL Plasmonic Nano-Arrays for Ultrasensitive Bio-Sensing. Nanophotonics 2018, 7, 1517–1531.

(7). Jackman JA; Linardy E; Yoo D; Seo J; Ng W; Klemme DJ; Wittenberg NJ; Oh S; Cho N Plasmonic Nanohole Sensor for Capturing Single Virus-Like Particles toward Virucidal Drug Evaluation. Small 2016, 12, 1159–1166. [PubMed: 26450658]

(8). Gérard D; Wenger J; Bonod N; Evgeni P; Rigneault H; Mahdavi F; Blair S; Dintinger J; Ebbesen TW Nanoaperture-Enhanced Fluorescence : Towards Higher Detection Rates with Plasmonic Metals. Phys. Rev. B 2008, 77, 045413.

(9). Wenger J; Conchonaud F; Dintinger J; Wawrezinieck L; Ebbesen TW; Rigneault H; Marguet D; Lenne P Diffusion Analysis within Single Nanometric Apertures Reveals the Ultrafine Cell Membrane Organization. Biophys. J 2007, 92, 913–919. [PubMed: 17085499]

(10). Zhao Y; Saleh AAE; Dionne JA Enantioselective Optical Trapping of Chiral Nanoparticles with Plasmonic Tweezers. ACS Photonics 2016, 3, 304–309.

(11). Jensen RA; Huang I; Chen O; Choy JT; Bischof TS; Lončar M; Bawendi MG Optical Trapping and Two-Photon Excitation of Colloidal Quantum Dots Using Bowtie Apertures. ACS photonics 2016, 3, 423–427.

(12). Yoo D; Gurunatha KL; Choi H; Mohr DA; Ertsgaard CT; Gordon R; Oh S Low-Power Optical Trapping of Nanoparticles and Proteins with Resonant Coaxial Nanoaperture Using 10 Nm Gap. Nano Lett. 2018, 18, 3637–3642. [PubMed: 29763566]

(13). Kim J; Lee Y Trapping of a Single DNA Molecule Using Nanoplasmonic Structures for Biosensor Applications. Biomed. Opt. Express 2014, 5, 2471–2480. [PubMed: 25136478]

(14). Kotnala A; Gordon R Double Nanohole Optical Tweezers Visualize Protein P53 Suppressing Unzipping of Single DNA-Hairpins. Biomed. Opt. Express 2014, 5, 1886–1894. [PubMed: 24940547]

(15). Lu G; Li W; Zhang T; Yue S; Liu J; Hou L; Li Z; Gong Q Plasmonic-Enhanced Molecular Fluorescence within Isolated Bowtie Nano-Apertures. ACS Nano 2012, 6, 1438–1448. [PubMed: 22247937]

(16). Regmi R; Balushi A. A. Al; Rigneault H; Gordon R; Wenger J Nanoscale Volume Confinement and Fluorescence Enhancement with Double Nanohole Aperture. Sci. Rep 2015, 5, 15852. [PubMed: 26511149]

(17). Wenger J; Dintinger J; Bonod N; Popov E; Lenne P-F; Ebbesen TW; Rigneault H Raman Scattering and Fluorescence Emission in a Single Nanoaperture : Optimizing the Local Intensity Enhancement. Opt. Commun 2006, 267, 224–228.

(18). Wenger J; Gérard D; Dintinger J; Mahboub O; Bonod N; Popov E; Ebbesen TW; Rigneault H Emission and Excitation Contributions to Enhanced Single Molecule Fluorescence by Gold Nanometric Apertures. Opt. Express 2008, 16, 3008–3020. [PubMed: 18542387]

(19). Ghenuche P; Torres J de; Moparthi, S. B.; Grigoriev, V.; Wenger, J. Nanophotonic Enhancement of the Förster Resonance Energy-Transfer Rate with Single Nanoapertures. Nano Lett. 2014, 14, 4707–4714. [PubMed: 25020141]

(20). Torres J. de; Ghenuche P; Moparthi BM; Grigoriev V; Wenger J FRET Enhancement in Aluminum Zero-Mode Waveguides. ChemPhysChem 2015, 16, 782–788. [PubMed: 25640052]

(21). Schön P; Bonod N; Devaux E; Wenger J; Rigneault H; Ebbesen TW; Brasselet S Enhanced Second-Harmonic Generation from Individual Metallic Nanoapertures. Opt. Lett 2010, 35, 4063–4065. [PubMed: 21124613]

(22). Lesuffleur A; Kumar LKS; Gordon R Apex-Enhanced Second-Harmonic Generation by Using Double-Hole Arrays in a Gold Film. Phys. Rev. B 2007, 75, 05423.

(23). Djaker N; Hostein R; Devaux E; Ebbesen TW; Rigneault H; Wenger J Surface Enhanced Raman Scattering on a Single Nanometric Aperture. J. Phys. Chem. C 2010, 114, 16250–16256.

(24). Brolo AG; Arctander E; Gordon R; Leathem B; Kavanagh KL Nanohole-Enhanced Raman Scattering. Nano Lett. 2004, 4, 2015–2018.

(25). Zhang X; Salcedo WJ; Rahman MM; Brolo AG Surface-Enhanced Raman Scattering from Bowtie Nanoaperture Arrays. Surf. Sci 2018, 676, 39–45.

(26). Ebbesen TW; Lezec HJ; Ghaemi HF; Thio T; Wolff PA Extraordinary Optical Transmission through Sub-Wavelength Hole Arrays. Nature 1998, 391, 667–669.

(27). Pang Y; Gordon R Optical Trapping of a Single Protein. Nano Lett. 2012, 12, 402–406. [PubMed: 22171921]

(28). Balushi A. A. Al; Gordon R Label-Free Free-Solution Single-Molecule Protein − Small Molecule Interaction Observed by Double-Nanohole Plasmonic Trapping. ACS photonics 2014, 1, 389–393.

(29). Kotnala A; Gordon R Double Nanohole Optical Tweezers Visualize Protein P53 Suppressing Unzipping of Single. Biomed. Opt. Express 2014, 5, 1886–1894. [PubMed: 24940547]

(30). Wheaton S; Gordon R Molecular Weight Characterization of Single Globular Proteins Using Optical Nanotweezers. Analyst 2015, 140, 4799–4803. [PubMed: 25739349]

(31). Blanchard-Dionne A-P; Meunier M Sensing with Periodic Nanohole Arrays. Adv. Opt. photonics 2017, 9, 891–940.

(32). Ferreira J; Santos MJL; Rahman MM; Brolo AG; Gordon R; Sinton D; Girotto EM Attomolar Protein Detection Using In-Hole Surface Plasmon Resonance. J. Am. Chem. Soc 2009, 131, 436–437. [PubMed: 19140784]

(33). Wheaton S; Gelfand RM; Gordon R Probing the Raman-Active Acoustic Vibrations of Nanoparticles with Extraordinary Spectral Resolution. Nat. Photonics 2014, 9, 68–72.

(34). Jones S; Balushi A. A. Al; Gordon R Raman Spectroscopy of Single Nanoparticles in a Double-Nanohole Optical Tweezer System. J. Opt 2015, 17, 102001.

(35). Zehtabi-oskuie A; Zinck AA; Gelfand RM; Gordon R Template Stripped Double Nanohole in a Gold Film for Nano-Optical Tweezers. Nanotechnology 2014, 25, 495301. [PubMed: 25407447]

(36). Ravindranath AL; Mirali Seyed S; Mathew S; Gordon R Colloidal Lithography Double-Nanohole Optical Trapping of Nanoparticles and Proteins. Opt. Express 2019, 27, 16184–16194. [PubMed: 31163802]

(37). Martin WE; Ge N; Srijanto BR; Furnish E; Collier CP; Trinkle CA; Richards CI Real-Time Sensing of Single-Ligand Delivery with Nanoaperture-Integrated Microfluidic Devices. ACS Omega 2017, 2, 3858–3867. [PubMed: 28782052]

(38). Raza MU; Peri SSS; Ma L-C; Iqbal SM; Alexandrakis G Self-Induced Back Action Actuated Nanopore Electrophoresis (SANE). Nanotechnology 2018, 29, 435501. [PubMed: 30073973]

(39). Aporvari MS; Kheirandish F; Volpe G Optical Trapping and Control of a Dielectric Nanowire by a Nanoaperture. Opt. Lett 2015, 40, 4807–4810. [PubMed: 26469625]

(40). Fauci AS; Pantaleo G; Stanley S; Weissman D Immunopathogenic Mechanisms of HIV Infection. Ann. Intern. Med 1996, 124, 654–663. [PubMed: 8607594]

(41). Pan Y-L; Wang C; Hill SC; Coleman M; Beresnev LA; Santarpia JL Trapping of Individual Airborne Absorbing Particles Using a Counterflow Nozzle and Photophoretic Trap for Continuous Sampling and Analysis. Appl. Phys. Lett 2014, 104, 113507.

(42). Kotnala A; Zheng Y; Fu J; Cheng W Microfluidic-Based High-Throughput Optical Trapping of Nanoparticles. Lab Chip 2017, 17, 2125–2134. [PubMed: 28561826]

(43). Shi X; Verschueren DV; Dekker C Active Delivery of Single DNA Molecules into a Plasmonic Nanopore for Label-Free Optical Sensing. Nano Lett. 2018, 18, 8003–8010. [PubMed: 30460853]

(44). Verschueren DV; Pud S; Shi X; De Angelis L; Kuipers L; Dekker C Label-Free Optical Detection of DNA Translocations through Plasmonic Nanopores. ACS Nano 2019, 13, 61–70. [PubMed: 30512931]

(45). Ndukaife JC; Kildishev AV; Nnanna AGA; Shalaev VM; Wereley ST; Boltasseva A Long-Range and Rapid Transport of Individual Nano-Objects by a Hybrid Electrothermoplasmonic Nanotweezer. Nat. Nanotechnol 2016, 11, 53–59. [PubMed: 26524398]

(46). Garcia-Guirado J; Rica RA; Ortega J; Medina J; Sanz V; Ruiz-Reina E; Quidant R Overcoming Diffusion-Limited Biosensing by Electrothermoplasmonics. ACS photonics 2018, 5, 3673–3679.

(47). Ndukaife JC; Xuan Y; George A; Nnanna AGA; Kildishev AV; Shalaev VM; Wereley ST; Boltasseva A High-Resolution Large-Ensemble Nanoparticle Trapping with Multifunctional Thermoplasmonic Nanohole Metasurface. ACS Nano 2018, 12, 5376–5384. [PubMed: 29847087]

(48). Sheehan PE; Whitman LJ Detection Limits for Nanoscale Biosensors. Nano Lett. 2005, 5, 803–807. [PubMed: 15826132]

(49). Yusupov VI; Tsypina SI; Bagratashvili VN Trapping of Nanoparticles in a Liquid by Laser-Induced Microbubbles. Laser Phys. Lett 2014, 11, 11.

(50). Yamamoto Y; Shimizu E; Nishimura Y; Iida T; Tokonami S Development of a Rapid Bacterial Counting Method Based on Photothermal Assembling. Opt. Mater. express 2016, 6, 1280–1285.

(51). Lin L; Peng X; Mao Z; Li W; Yogeesh MN; Rajeeva BB; Perillo EP; Dunn AK; Akinwande D; Zheng Y Bubble-Pen Lithography. Nano Lett. 2016, 16, 701–708. [PubMed: 26678845]

(52). Liu GL; Kim J; Lu YU; Lee LP Optofluidic Control Using Photothermal Nanoparticles. Nat. Mater 2005, 5, 27–32. [PubMed: 16362056]

(53). Setoura K; Ito S; Miyasaka H Stationary Bubble Formation and Marangoni Convection Induced by CW Laser Heating of a a Single Gold Nanoparticle. Nanoscale 2017, 9, 719–730. [PubMed: 27959376]

(54). Miaoa X; Wilson BK; Lin LY Localized Surface Plasmon Assisted Microfluidic Mixing. Appl. Phys. Lett 2008, 92, 124108.

(55). Donner JS; Baffou G; McCloskey D; Quidant R Plasmon-Assisted Optofluidics. ACS Nano 2011, 5, 5457–5462. [PubMed: 21657203]

(56). Roxworthy BJ; Bhuiya AM; Vanka SP; Toussaint KC Understanding and Controlling Plasmon-Induced Convection. Nat. Commun 2014, 5, 3173. [PubMed: 24445431]

(57). Wang K; Schonbrun E; Steinvurzel P; Crozier KB Trapping and Rotating Nanoparticles Using a Plasmonic Nano-Tweezer with an Integrated Heat Sink. Nat. Commun 2011, 2, 469. [PubMed: 21915111]

(58). Jiang Q; Rogez B; Claude J-B; Baffou G; Wenger J Temperature Measurement in Plasmonic Nanoapertures Used for Optical Trapping. ACS Photonics 2019, 6, 1763–1773.

(59). Xu Z; Song W; Crozier KB Direct Particle Tracking Observation and Brownian Dynamics Simulations of a Single Nanoparticle Optically Trapped by a Plasmonic Nanoaperture. ACS Photonics 2018, 5, 2850–2859.

(60). Soares Martins T; Catita J; Martins Rosa I; A. B. da Cruz e Silva O; Henriques AG Exosome Isolation from Distinct Biofluids Using Precipitation and Column-Based Approaches. PLoS One 2018, 13, e0198820. [PubMed: 29889903]

(61). Heider S; Metzner C Quantitative Real-Time Single Particle Analysis of Virions. Virology 2014, 462–463, 199–206.

(62). Rusling JF; Kumar CV; Gutkind JS; Patel V Measurement of Biomarker Proteins for Point-of-Care Early Detection and Monitoring of Cancer. Analyst 2010, 135, 2496–2511. [PubMed: 20614087]

(63). Rodríguez LM; Gayone JE; Sánchez EA; Grizzi O; Blum B; Salvarezza RC; Xi L; Lau WM Gas Phase Formation of Dense Alkanethiol Layers on GaAs(110). J. Am. Chem. Soc 2007, 129, 7807–7813. [PubMed: 17550246]

(64). Ito E; Noh J; Hara M Steric Effects on Adsorption and Desorption Behaviors of Alkanethiol Self-Assembled Monolayers on Au(111). Chem. Phys. Lett 2008, 462, 209–212.

(65). Stettner J; Frank P; Griesser T; Trimmel G; Schennach R; Gilli E; Winkler A A Study on the Formation and Thermal Stability of 11-MUA SAMs on Au(111)/Mica and on Polycrystalline Gold Foils. Langmuir 2009, 25, 1427–1433. [PubMed: 19119802]

(66). Prasad A; Choi J; Jia Z; Park S; Gartia MR Nanohole Array Plasmonic Biosensors: Emerging Point-of-Care Applications. Biosens. Bioelectron 2019, 130, 185–203. [PubMed: 30738247]

(67). Li J; Hill EH; Lin L; Zheng Y Optical Nanoprinting of Colloidal Particles and Functional Structures. ACS Nano 2019, 13, 3783–3795. [PubMed: 30875190]

(68). Peng X; Lin L; Hill EH; Kunal P; Humphrey SM; Zheng Y Optothermophoretic Manipulation of Colloidal Particles in Nonionic Liquids. J. Phys. Chem. C 2018, 122, 24226–24234.

(69). Lin L; Hill EH; Peng X; Zheng Y Optothermal Manipulations of Colloidal Particles and Living Cells. Acc. Chem. Res 2018, 51, 1465–1474. [PubMed: 29799720]

(70). Li J; Lin L; Inoue Y; Zheng Y Opto-Thermophoretic Tweezers and Assembly. J. Micro Nano-Manufacturing 2018, 6, 1–10.

(71). Lin L; Lepeshov S; Krasnok A; Jiang T; Peng X; Korgel BA; Alù A; Zheng Y All-Optical Reconfigurable Chiral Meta-Molecules. Mater. Today 2019, 25, 10–20.

(72). Peng X; Li J; Lin L; Liu Y; Zheng Y Opto-Thermophoretic Manipulation and Construction of Colloidal Superstructures in Photocurable Hydrogels. ACS Appl. Nano Mater. 2018, 1, 3998–4004. [PubMed: 31106296]

(73). Johnson PB; Christy RW Optical Constants of the Noble Metals. Phys. Rev. B 1972, 6, 4370–4379.

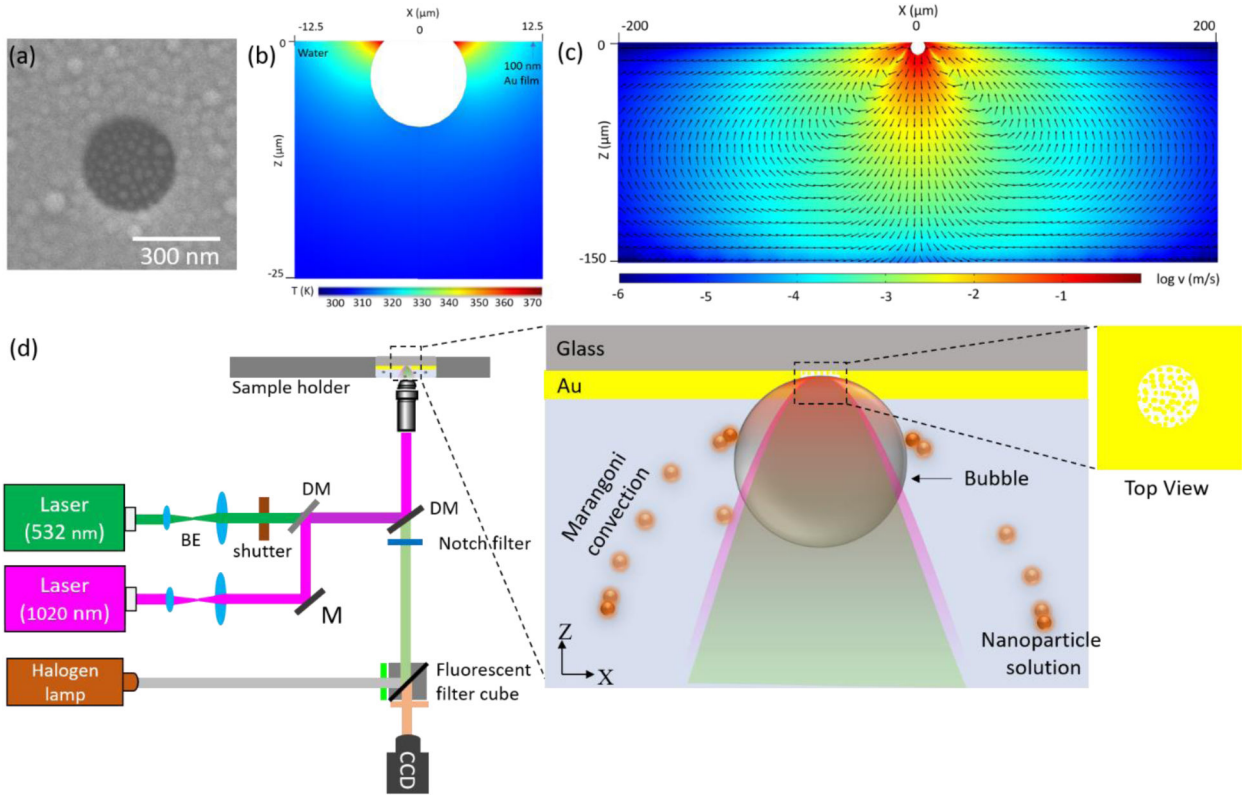

Figure 1.

Bubble-assisted trapping using AuNIs-encapsulated nanoaperture (a) Scanning electron microscope (SEM) image of an AuNIs-encapsulated nanoaperture of a diameter of 300 nm on a 100 nm-thick Au film. (b) Cross-sectional view of the simulated temperature distribution around a 10 μm bubble generated at an AuNIs-encapsulated nanoaperture. (c) Cross-sectional view of the simulated flow velocity distribution around a 10 μm bubble. (d) Schematic of the experimental set-up for bubble-assisted trapping. The enlarged section shows the AuNIs-encapsulated nanoaperture with the bubble and the induced flow in the solution chamber. DM: Dichroic mirror, BE: Beam expander, M: Mirror, CCD: Charge-coupled device.

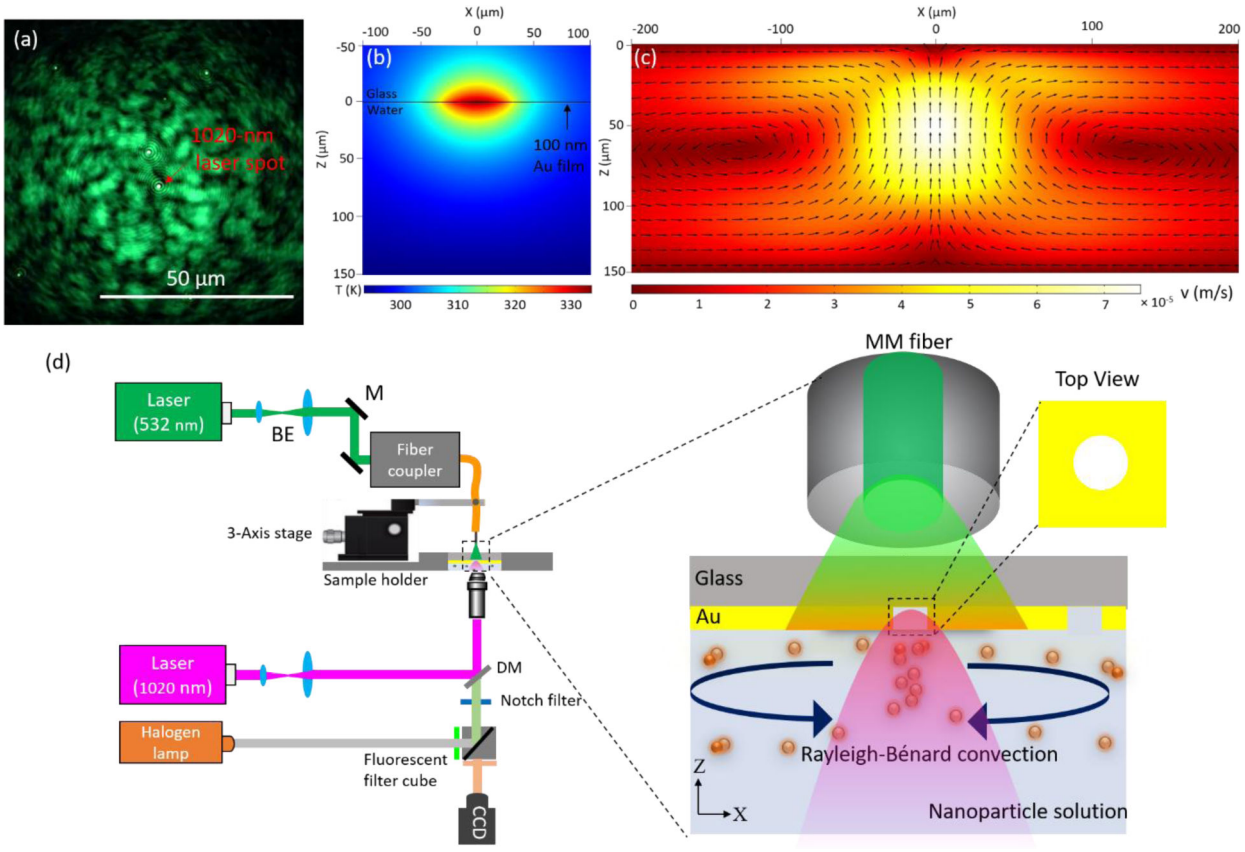

Figure 2.

Convection-assisted trapping (a) Optical microscope image showing the illumination of large area (diameter ~ 60 µm) surrounding a single nanoaperture using a multimode (MM) optical fiber. The arrow points to the nanoaperture used for trapping of particles and excited with a laser of a wavelength of 1020 nm. (b) Cross-sectional view of the simulated temperature distribution around a single nanoaperture on a 100 nm Au film (c) Cross-sectional view of the simulated convection flow velocity distribution around the nanoaperture. (d) Schematic of the experimental set-up for convection-assisted trapping. The enlarged section shows a MM fiber illuminating a large area around a single nanoaperture and the Rayleigh-Bénard convection inducing flow in the solution chamber. DM: Dichroic mirror, BE: Beam expander, M: Mirror, CCD: Charge-coupled device.

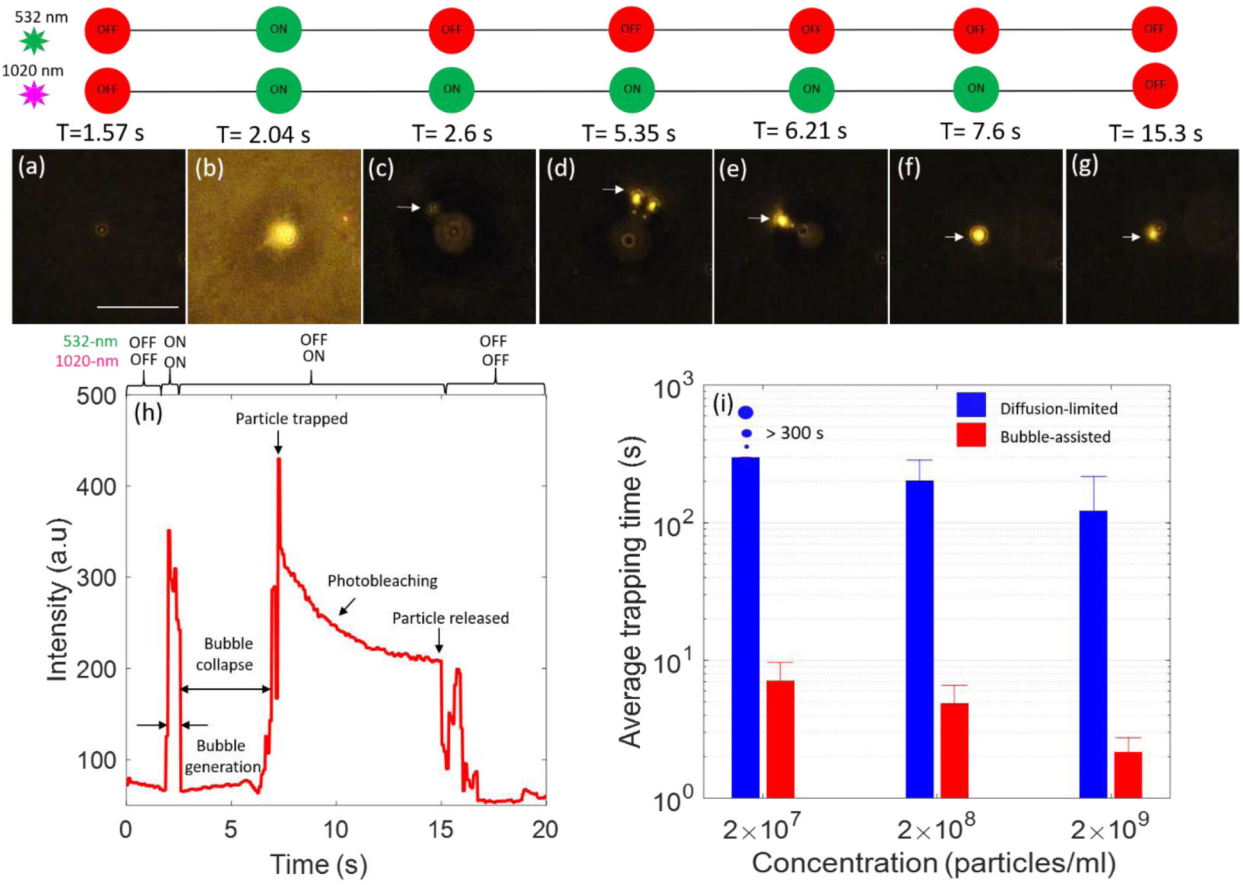

Figure 3.

Bubble-assisted trapping (a–g)Time-lapse images of bubble-assisted trapping showing bubble generation, bubble collapse and trapping & release of a single 200 nm fluorescent polystyrene nanoparticle using an AuNIs-encapsulated circular nanoaperture. The arrow points to the 200 nm polystyrene particle. Scale bar: 10 μm. (h) Time trace of intensity at the nanoaperture during the bubble-assisted trapping process shown in Figures 3 (a–g) (Supporting Video 3). (i) Comparison of the average particle-trapping time measured for diffusion-limited and bubble-assisted traps at different particle concentrations. The bar height and the error bars represent the mean and standard deviation for sample size of N=24, 23 and 20 for bubble-assisted trapping and N=12, 4 and 3 for diffusion-limited trapping at concentrations of 2×10^9, 2×10^8 and 2×10^7 particles/ml, respectively.

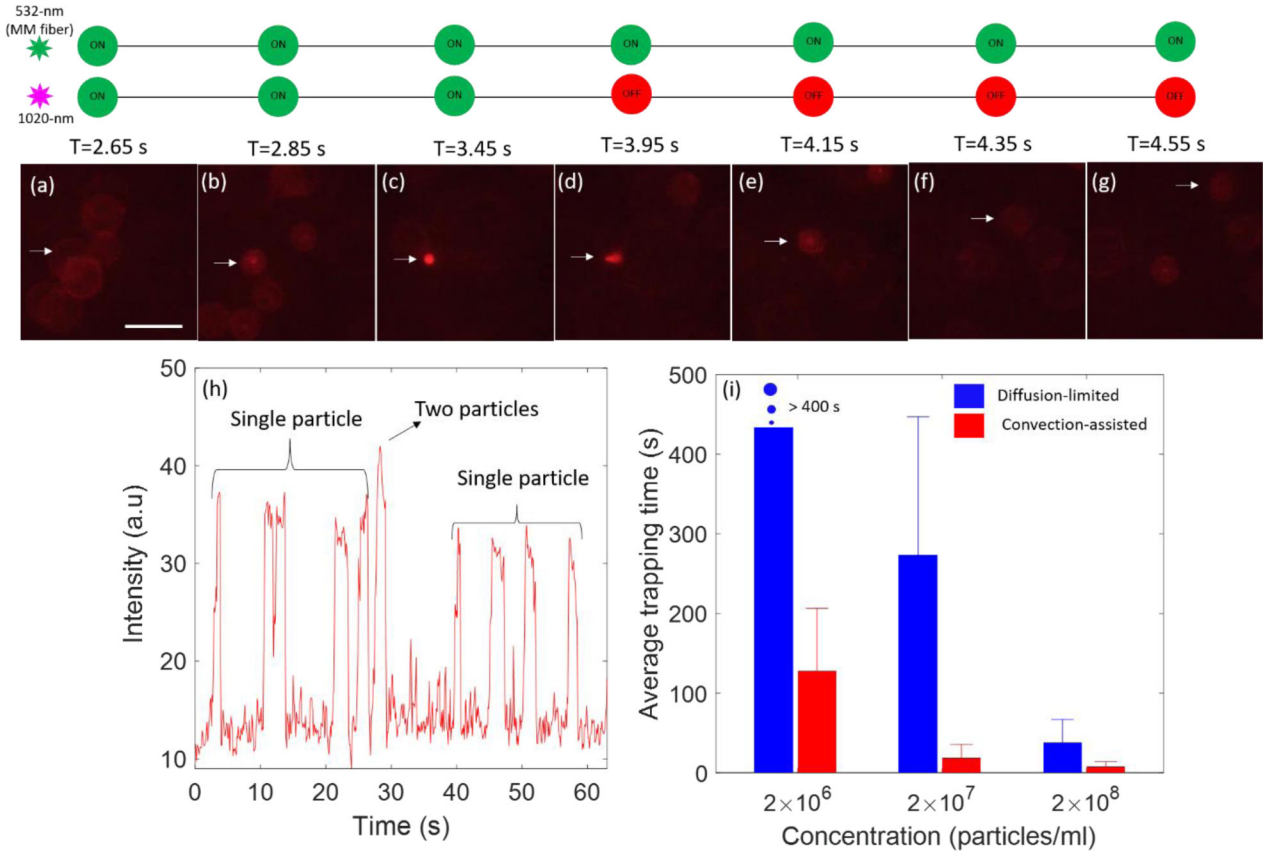

Figure 4.

Convection-assisted trapping (a–g) Time-lapse images of convection-assisted trapping showing the Rayleigh-Bénard convection flow and trapping of a single 200 nm fluorescent polystyrene nanoparticle using an AuNIs-encapsulated circular nanoaperture. The time-lapse images correspond to the first trapping event shown in Figure 4h. Scale bar: 25 μm. (h) Time trace of intensity at the nanoaperture during the convection-assisted trapping process shown in Supporting Video 6. (i) Comparison of the average trapping time measured from diffusion-limited and convection-assisted traps at concentrations of 2×10^8, 2×10^7 and 2×10^6 particles/ml. The bar height and the error bars represent the mean and standard deviation for sample size of N=68, 40 and 14 for convection-assisted and N=27, 12 and 3 for diffusion-limited trapping at concentrations of 2×10^8, 2×10^7 and 2×10^6 particles/ml, respectively.

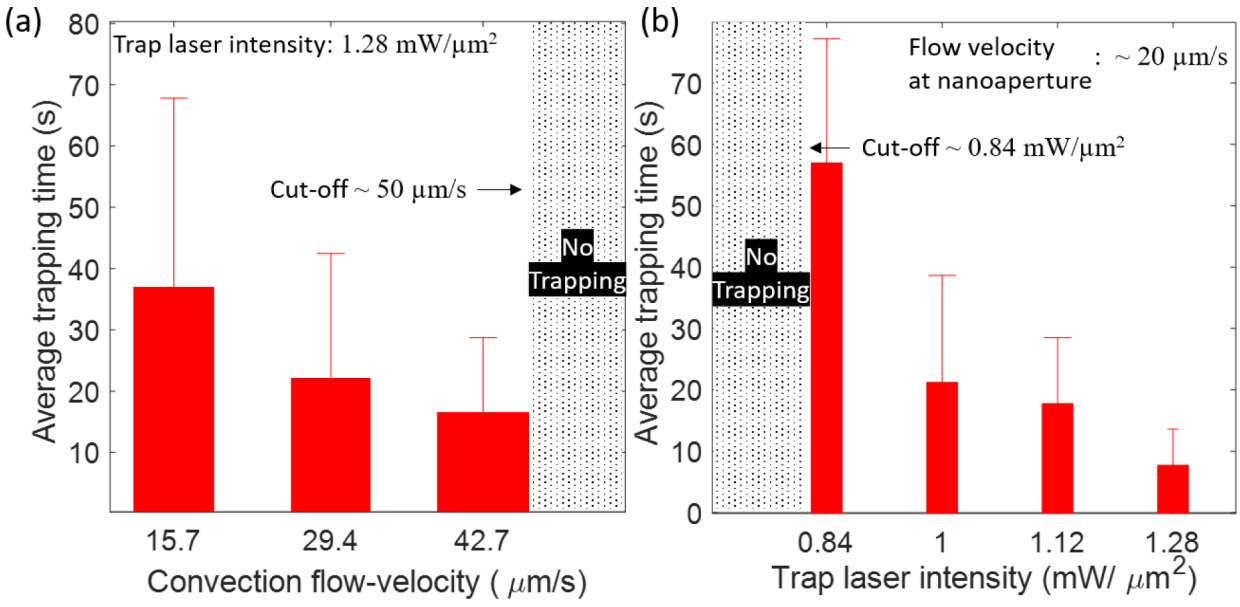

Figure 5.

Effect of flow velocity and trap laser power in a convection-assisted trap (a) Impact of convection flow velocity on the average particle-trapping time in a convection-assisted trap. The bar height and the error bars represent the mean and standard deviation for sample size of N=28, N=73 and N=118 for mean convection flow velocity of 15.7, 29.4 and 42.7 μm/s, respectively. The width of the bar corresponds to the standard deviation of the convection-flow velocities. (b) Impact of trap laser power on the average particle-trapping time in a convection-assisted trap. The bar height and the error bars represent mean and standard deviation for sample size of N=3, N=27, N=34 and N=68 for trap laser intensity of 0.84, 1, 1.12 and 1.28, respectively.

Table 1:

A summary of comparison of sample design, flow mechanism and trapping process of bubble- and convection-assisted trap.

	Bubble-assisted trap	**Convection-assisted trap**
Sample design	AuNIs-encapsulated nanoapertures	Simple nanoapertures on Au films
Flow mechanism	Marangoni convection	Rayleigh-Bénard convection
Trapping process	Discrete	Continuous